Advances in Materials Technology for Fossil Power Plants
Proceedings from the Eighth International Conference
October 11–14, 2016, Albufeira, Algarve, Portugal
https://doi.org/10.31399/asm.cp.am-epri-2016p0149

CREEP-FATIGUE LIFE AND DAMAGE EVALUATION OF NI-BASED ALLOY 617 AND ALLOY 740H

Shengde Zhang and Yukio Takahashi
Central Research Institute of Electric Power Industry, 2-6-1 Nagasaka, Yokosuka-shi, Kanagawa-ken 240-0196 Japan

ABSTRACT

Creep-fatigue lives of nickel-based Alloy 617 and Alloy 740H were investigated to evaluate their applicability to advanced ultrasupercritical (A-USC) power plants. Strain controlled push-pull creep-fatigue tests were performed using solid bar specimen under triangular and trapezoidal waveforms at 700°C. The number of cycles to failure was experimentally obtained for both alloys and the applicability of three representative life prediction methods was studied.

INTRODUCTION

For enhancement of thermal efficiency and reduction of CO_2 emission in coal-fired power plants, advanced ultra-supercritical (A-USC) power plant in which steam temperature is raised from 600°C in the conventional USC power plants to 700°C or higher, is under development as a worldwide activity [1-2]. Conventional ferritic and austenitic steels cannot fulfill the requirement of creep strength at these temperatures and Ni-based alloys have emerged as principal candidates due to their excellent creep strength, better oxidation and corrosion resistance. Alloy 617 and Alloy 740H are currently considered as two leading candidate materials for boiler tubing and piping in A-USC power plant [3-5]. Many studies have been extensively performed for microstructure stability [6-8], tensile properties [9] and creep strength of base metal and welded joints [10-11] for evaluating long-term structural integrity.

In structural design and life management of fossil power plants, failure due to a combined effect of fatigue and creep damages often becomes an important phenomenon to be considered, which arises due to startup and shutdown or power transients during normal operation of the plant. In addition, the coefficient of thermal expansion of Ni-based alloys is larger than those of ferritic steels, which results in higher thermal stress compared with USC plants, particularly in thick-walled components. Knowledge of creep-fatigue behavior as well as creep strength is important for design and life management of A-USC power plant. However, there are few experimental studies on the creep-fatigue behavior of both Alloy 617 and Alloy 740H and no systematic effort has been made for developing design and life evaluation procedures.

The objective of this paper is to study the creep-fatigue behavior of Alloy 617 and Alloy 740H, for evaluating its applicability to A-USC power plants. Strain controlled push-pull creep-fatigue tests were performed using solid bar specimen under triangular and trapezoidal waveforms at 700°C. The number of cycles to failure was experimentally obtained and the effect of strain hold time was studied. In addition, three creep-fatigue damage rules were applied to the experimental data: time fraction rule (TFR), ductility exhaustion model (DEM) and modified ductility exhaustion model (MDEM) to evaluate their performances.

EXPERIMENTAL PROCEDURE

The materials tested were Alloy 617 piping (308mmOD×80mmt×200mmL) and Alloy 740H piping (205mmID×72.5mmt×150mmL). Both materials were provided by Daido Special Metals. Chemical compositions and heat treatment of both materials are listed in Table 1. Compared with old version [5], Alloy 617 used in this study is within narrower tolerances of alloying elements (Cr, Fe, Co, Al and Ti) and additions of B to increase creep strength [5]. Alloy 740H is a relatively new Ni-based superalloy modified on the basis of Alloy 740 to improve the structural stability [3]. Alloy 617 was subjected to solution annealed at 1163°C for 1.75 hours followed by water quenching but no additional heat treatment for aging, whereas Alloy 740H was received in solution annealed and aged condition following the ASME Code Case 2702. Figure 1 shows microstructures of as-received alloys. As shown in Fig. 1(a), there were no γ' phase precipitates within grains but discontinuously precipitated carbides were observed along grain boundaries in Alloy 617. On the other hand, fine γ' phase precipitates with a diameter of about 20nm were observed within grain interiors as well as relatively large carbides along grain boundaries in Alloy 740H as shown in Fig. 1(b).

Round bar specimens whose diameter and length at the test section were 8mm and 16mm, was used in this study. Their geometry and dimensions are shown in Fig. 2, where the gage length for strain measurement was 12.5mm. The axis of the specimen was aligned to axial direction of the piping. Electric-mechanical uniaxial fatigue machines (Instron 8861) were used. Temperatures of the specimens were raised by an electric resistance furnace and the temperature variation in the gage section was kept within ±3°C during the tests.

Table 1: Chemical compositions of both materials tested (wt%).

	C	B	Cr	Mo	Co	Al
Alloy 617	0.07	0.004	22.35	9.48	11.53	1.03
Alloy 740H	0.045	-	24.7	0.006	20.2	1.33
	Ti	Nb	Mn	Fe	Si	Ni
Alloy 617	0.42	-	0.04	0.43	0.03	Bal.
Alloy 740H	1.36	1.52	0.246	0.238	0.137	Bal.

Alloy 617: Solution annealed (1163℃×1.75h), WQ, Alloy 740H: Solution annealed and aged

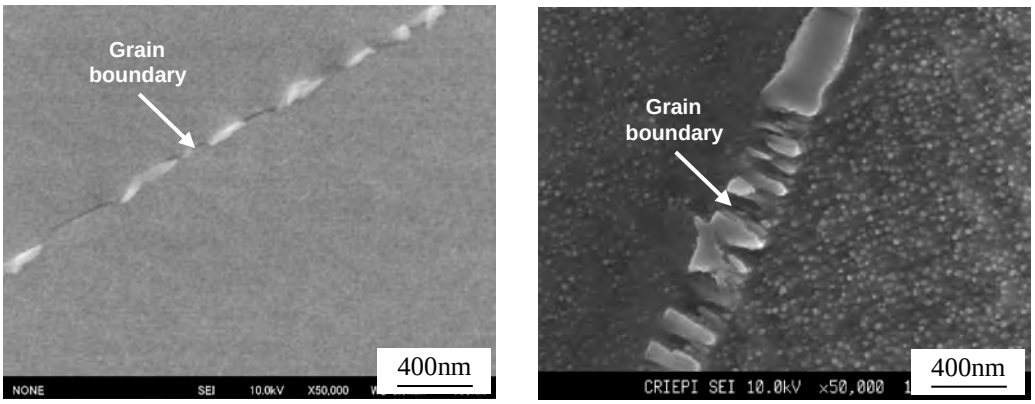

(a) Alloy 617 (b) Alloy 740H

Figure 1: Microstructure of the material tested.

Strain controlled tests were conducted under two strain waveforms shown in Fig. 3 at 700°C. Figure 3(a) is a fully reversed symmetrical triangular strain wave with a strain rate of 0.1%/s (pure fatigue test), whereas Fig. 3(b) is a trapezoidal waveform introducing the hold time at tensile peak strain. The number of cycles to failure (N_f) was defined as the cycle of 25% drop of tensile peak stress from that at the half life.

RESULTS AND DISCUSSION

Creep-Fatigue Life

Figure 4 shows the variation of maximum and minimum stresses with number of cycles in the tests without hold time (pure fatigue tests) and with hold times from 0.1h to 5h. As shown in Fig. 4(a), Alloy 617 displayed clear cyclic hardening in all the loading conditions and compressive mean stresses were found in the tests with tensile hold times. As shown in Fig. 4(b), slight cyclic hardening was observed in the early cycles but the material exhibited a tendency to cyclically soften beyond about 10% of the life in the pure fatigue test of Alloy 740H. In the tests with tensile hold times, compressive mean stresses were observed and the maximum stresses were smaller than that in the pure fatigue test.

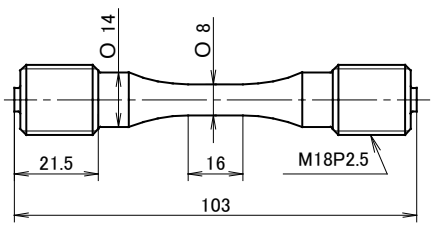

Figure 2: Shape and dimensions of specimen tested.

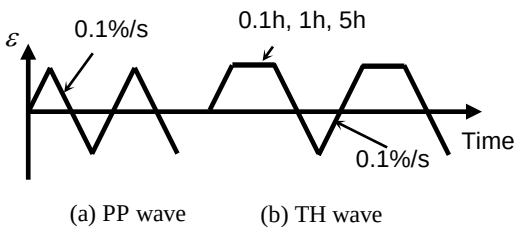

Figure 3: Strain waveforms

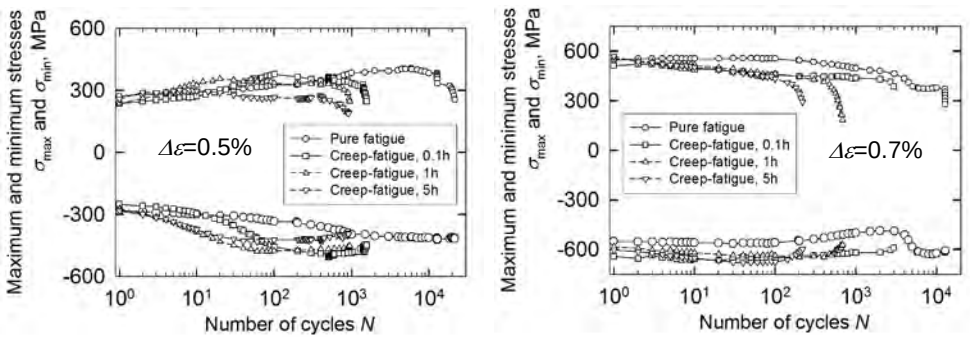

(a) Alloy 617 (b) Alloy 740H

Fig.4: Variation of maximum and minimum stresses with number of cycles.

Figure 5 presents the stress relaxation curves during hold time at total strain ranges of 1.0% and 0.5% with 1h hold time of Alloy 617. In this figure, white and black plots represent experimental results at first cycle and half life and solid line is the predicted curve based on creep equations representing primary, secondary and tertiary creep deformations under constant load [12]. It can be seen that stress relaxation curves at half life cycle are much lower than those at the first cycle at both strain ranges. The predicted curve was lower than the experimental date at the first cycle and close to the half life cycle at total strain range of 1.0%, Fig. 5(a), and was comparable to the first cycle response at total strain range of 0.5%, Fig. 5(b).

Figure 6 shows the stress relaxation curves during hold time at total strain ranges of 1.2% and 0.7% with 1h hold time of Alloy 740H. Regardless of the test conditions, stress was quickly relaxed in the first few minutes and relatively small stress relaxation followed in the remaining period. The rapid drop of stress after the initiation of strain hold is more significant at the half life than at the first cycle, which results in smaller stress during the hold time. This may result from the material softening due to the cyclic loading of Alloy 740H as shown in Fig. 4(b). Comparing the predicted curve with the experimental data, the rapid drop of stress cannot be expressed by the method based on original creep equation even at the first cycle. Takahashi [13] pointed out that stress relaxation behavior of a class of austenitic stainless steel is significantly influenced by the prior strain rate and proposed a concept of "viscous strain" to simulate the rapid drop of stress. Application of such an approach would be required for the present material also.

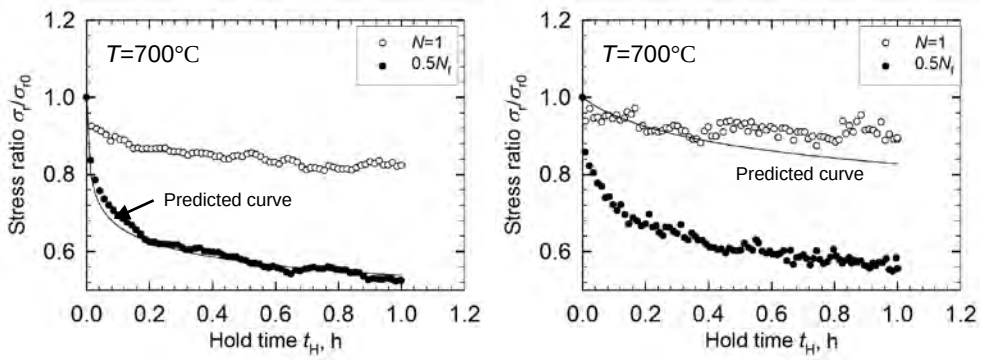

(a) $\Delta\varepsilon$ =1.0% (b) $\Delta\varepsilon$ =0.5%

Figure 5: Stress relaxation behaviors of Alloy 617.

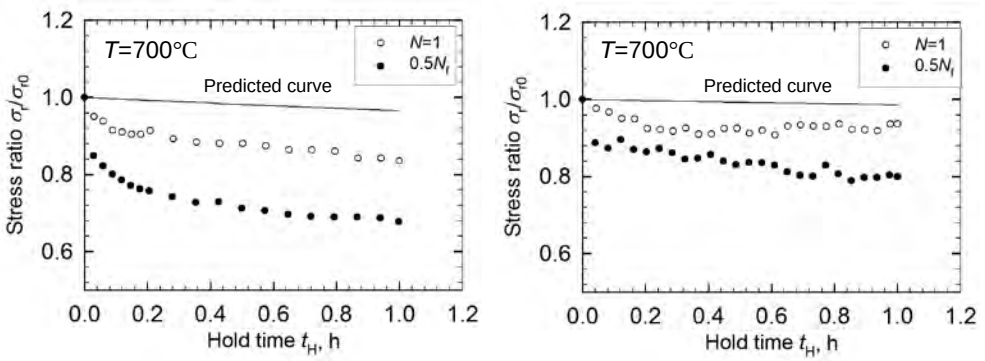

(a) $\Delta\varepsilon$ =1.2% (b) $\Delta\varepsilon$ =0.7%

Figure 6: Stress relaxation behaviors of Alloy 740H.

Figure 7 correlates the pure fatigue and creep-fatigue lives with total strain range for both materials. In the figure, solid lines are drawn based on the pure fatigue data of each material, and two dashed lines represent the life reduction factors of 5 and 50. Creep-fatigue lives are significantly smaller than pure fatigue lives in both alloys. Especially, the failure life in the creep-fatigue test with 5h hold time was down to a factor of 1/50 in both materials. Moreover, life reduction ratio at the small strain range was larger than that at the larger strain range, which is similar to other materials reported by Takahashi [13-14].

Figure 8 plots life ratio against the hold time at 0.5% for Alloy 617 and 0.7% for Alloy 740H, in comparison with conventional materials, Gr. 91 [14] and 316FR [15]. The life ratio monotonically decreased with the increase of hold time for all materials. Smaller life ratio was obtained in Alloy 617 and Alloy 740H than 316FR and Gr. 91. This result indicates that creep-fatigue life of Alloy 617 and Alloy 740H is more sensitive to the hold time during tensile peak strain holding than Gr. 91 and 316FR.

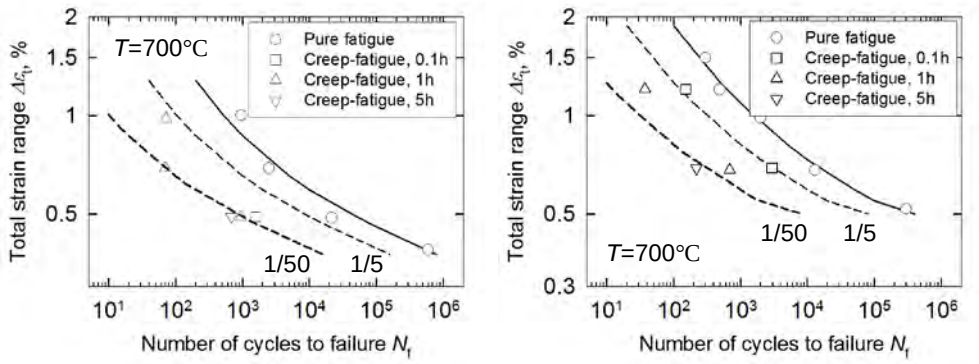

(a) Alloy 617 (b) Alloy 740H

Figure 7: Correlation of numbers of cycles to failure with total strain range.

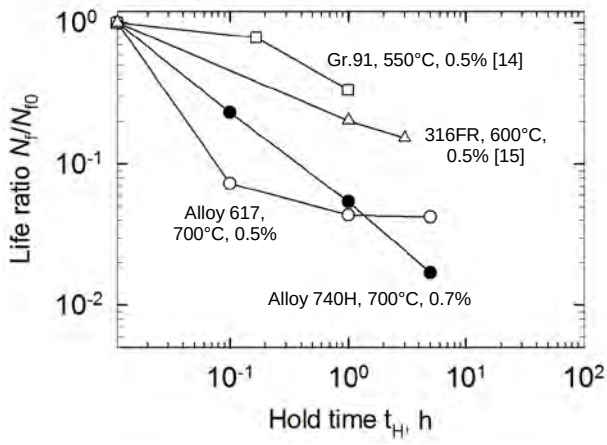

Figure 8: Creep-fatigue life reduction with hold time.

Figure 9 shows fracture surfaces observed after pure fatigue and creep-fatigue tests as representative cases. In the pure fatigue tests, crack initiated at surface and propagated macroscopically in the normal direction to the specimen axis. Transgranular fracture with clear striations morphology was observed as shown in Fig. 9(a) and (c). In contrast, almost the whole fracture surface was found to be intergranular in the creep-fatigue tests, Fig. 9(b) and (d), suggesting aninvolvement of large crack damage.

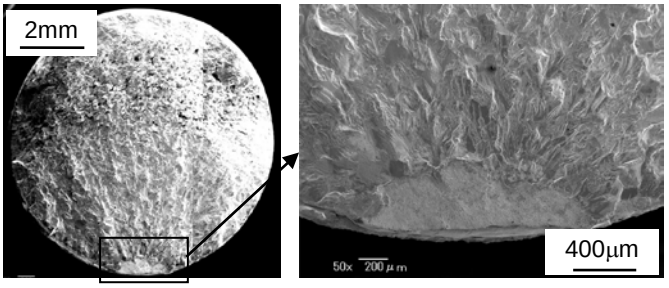

(a) Alloy 617, Pure fatigue, $\Delta\varepsilon_t$=0.4%

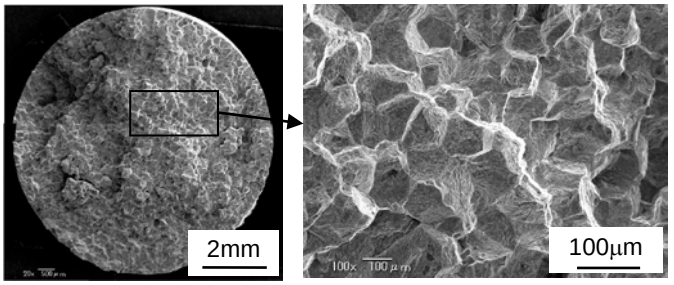

(b) Alloy 617, Creep-fatigue, $\Delta\varepsilon_t$=0.5%, 1h hold time

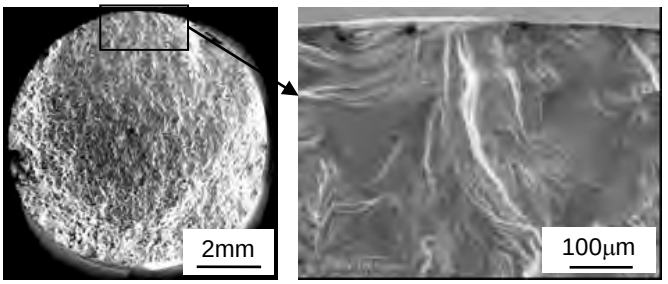

(c) Alloy 740H, Pure fatigue, $\Delta\varepsilon_t$=0.7%

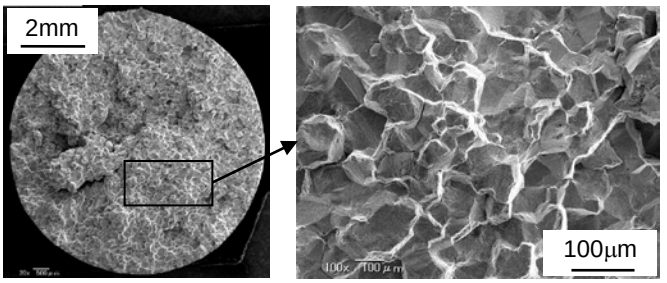

(d) Alloy 740H, Creep-fatigue, $\Delta\varepsilon_t$=0.7%, 1h hold time

Figure 9: Fracture surfaces observed after pure fatigue and creep-fatigue tests.

Creep-Fatigue Damage Rule

This study applied three representative creep-fatigue damage rules to examine their applicability to creep-fatigue life prediction of Alloy 617 and Alloy 740H. The damage rules applied were time fraction rule (TFR), ductility exhaustion model (DEM) and modified ductility exhaustion model (MDEM).

Time fraction rule is widely employed in the current design codes [16] for high temperature components. By this approach, creep damage per cycle was calculated using the following equation:

$$D_c = \int_0^{t_H} \frac{dt}{t_r(\sigma, T)} \tag{1}$$

where t_H is the hold time, t_r is the time to creep rupture at the stress, σ and temperature, T. Fatigue damage per cycle, D_f, is calculated as a reciprocal of the pure fatigue life, N_{f0}, at the same strain range, temperature and strain rate as those in the creep-fatigue tests as

$$D_f = \frac{1}{N_{f0}} \tag{2}$$

The simplest linear damage summation represented by a straight line connecting (1, 0) and (0, 1) in the interaction diagram was used in this study.

Figure 10 shows the correlation of times to creep rupture with applied stress at 700°C for both alloys [12]. Dashed and solid lines in the figure drawn based on the creep test data of Alloy 617 and Alloy 740H were used in calculation of the creep damage. Alloy 740H exhibits greater creep strength than Alloy 617, which may result from the different contents of γ' phase between both alloys.

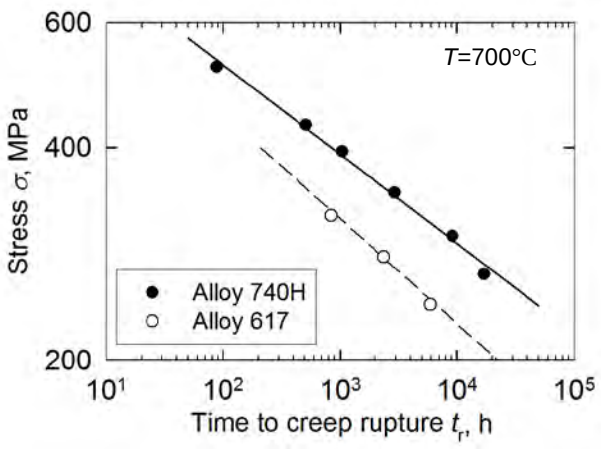

Figure 10: Correlation of times to creep rupture with stress.

Ductility exhaustion model developed mainly by researchers in the United Kingdom [17] has been receiving much attention in the viewpoint of application to long life components including fossil power plants. In this approach, creep damage is calculated by

$$D_c = \int_0^{t_H} \frac{\dot{\varepsilon}_c}{\delta} dt \tag{3}$$

where $\dot{\varepsilon}_c$ is creep strain rate, δ is the creep ductility. As a value of δ, various quantities such as rupture elongation, reduction of area and true fracture strain have been used depending on researchers and/or materials concerned. Moreover, its dependency on the creep strain rate is often taken into account. In this study, rupture elongation considering the dependency on the inelastic strain rate was used for each alloy. The fatigue damage and the failure criterion are the same as those used in the application of the time fraction rule.

Figure 11 plots the variation of rupture elongation with inelastic strain rate obtained in tensile and creep tests [12]. The rupture elongation of Alloy 740H in strain-controlled tensile test decreased with decreasing the inelastic strain rate and it took almost a constant value of about 5% in the creep testing region. The elongation of Alloy 617 decreased with decreasing the inelastic strain rate in the tensile test but re-increased in the creep tests. Alloy 617 shows the minimum ductility in the inelastic strain range of about 10^{-1}%/h. In the tensile tests at these strain rates, significant serration (dynamic aging) was observed on stress-strain curve, which may cause the reduction of ductility. However, Alloy 617 exhibited larger elongation compared with Alloy 740H, irrespective of the inelastic strain rate.

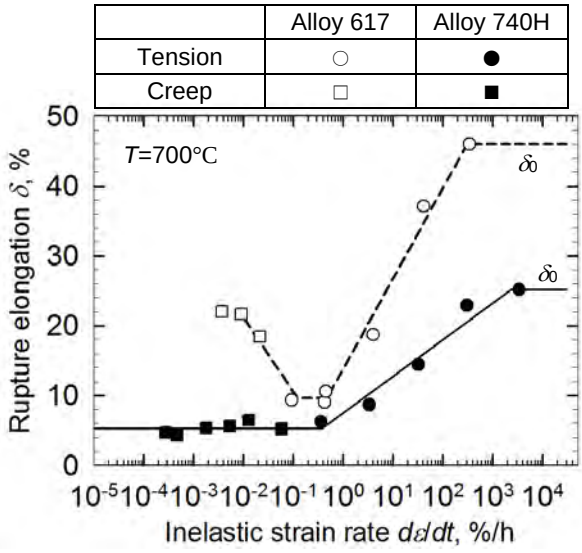

Figure 11: Relationship between rupture elongation and inelastic strain rate.

In the same way as the ramping periods of the cycles at relatively high strain rates are usually excluded from the evaluation of creep damage, inelastic deformation during an early portion of hold period may be less harmful than the latter portion because of its higher rate. In order to include this effect into life prediction, calculation of creep damage was changed in modified ductility exhaustion model as below [14, 18].

$$D_c = \int_0^{t_H} \left(\frac{1}{\delta} - \frac{1}{\delta_0}\right) \dot{\varepsilon}_c \, dt \tag{4}$$

δ_0 is the ductility obtained in the tests conducted at a sufficiently high strain rate and considered as creep damage free. Generally, the elongation obtained in the conventional tensile tests at the strain rate similar to that in pure fatigue tests is employed. In this study, the values of δ_0 were set to 46% and 25% for Alloy 617 and Alloy 740H as shown in Fig. 11.

Creep-Fatigue Damage Evaluation

Figure 12 compares the predicted lives according to TFR, DEM and MDEM with the experimental lives of both alloys. Experimental stress relaxation at half life and predicted curve were used in combinations with three life prediction approaches described above.

Based on the experimental stress relaxation, TFR overestimated the creep-fatigue lives for all conditions because of the small creep damage calculated, although some data are within a factor of 2. Especially, the lives of Alloy 617 were overestimated by a factor of 15. The reason for the underestimation of creep damage by TFR is perhaps that it does not take into account the transient creep strain generated at each cycle of the creep-fatigue tests. On the contrary, the creep-fatigue lives trended to be underestimated by DEM with a maximum factor of about 16, which was obtained by the test on Alloy 740H at a strain range of 0.7% and a hold time of 0.1h. The prediction was slightly improved by MDEM with maximum factor decreasing from 16 to 12.

Based on the predicted stress relaxation curves, on the other hand, the creep-fatigue lives of Alloy 740H were very accurately predicted by TFR within a factor of 2, but some lives of Alloy 617 were still overestimated. In contrast to the results based on experimental curve, DEM overestimated the lives of Alloy 740H for all test conditions and there was no large difference between DEM and MDEM. They are because only small amount of stress relaxation was predicted in all tests as shown in Fig. 6. The data of Alloy 617, on the other hand, were predicted almost within a factor of 2 by both DEM and MDEM. In addition the scatter of MDEM was smaller than that of DEM.

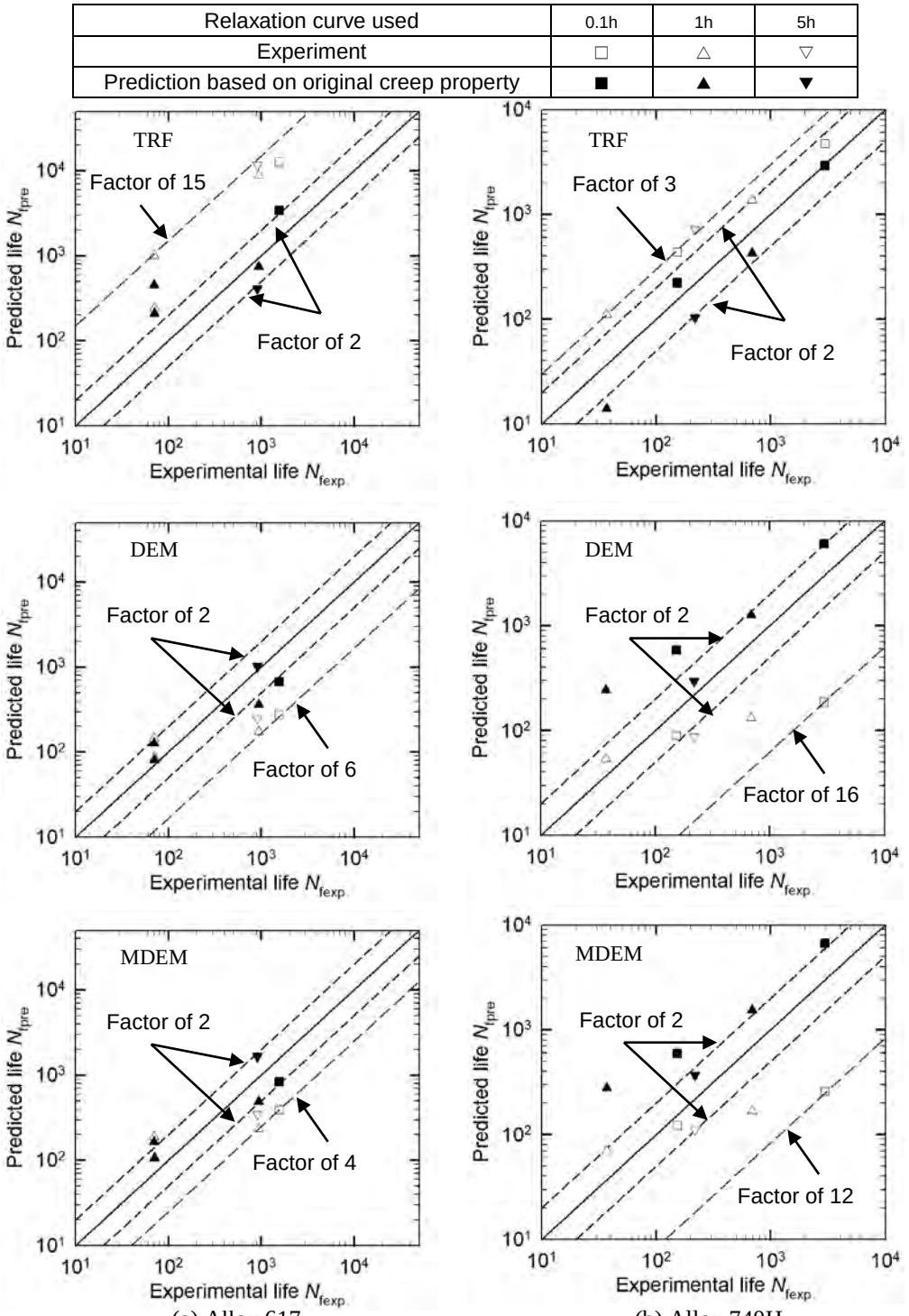

(a) Alloy 617 (b) Alloy 740H

Figure 12: Comparison of predicted lives with experimental lives.

SUMMARY

In the creep-fatigue test conditions, Alloy 617 exhibited cyclic hardening behavior whereas cyclic softening was found in Alloy 740H.

Creep-fatigue lives with hold time at tensile peak strain were smaller than those in the pure fatigue test for Alloy 617 and Alloy 740H and the creep-fatigue lives decreased with the increase of hold time. The life reduction ratio of both alloys was larger than that of conventional materials, Gr. 91 and 316FR.

Based on the experimental stress relaxation, time fraction rule overestimated the creep-fatigue lives of Alloy 617 and Alloy 740H with a factor of 15 and 3, respectively. Ductility exhaustion model underpredicted failure lives, giving the largest error by a factor of 16 and the prediction was improved by modified ductility exhaustion model only slightly. Based on the predicted stress relaxation, time fraction rule correlated the creep-fatigue lives of Alloy 740H within a factor of 2 and the data of Alloy 617 were accurately estimated by MDEM.

In summary, ratios of the predicted lives against the test data in creep-fatigue loading conditions have shown large variations, depending on the way to estimate creep damage and the selection of stress relaxation curves as well as material type. Much more efforts seem to be required for establishing a reliable procedure to predict the failure lives of these alloys under creep-fatigue interaction.

REFERENCES

[1] Fukuda, M., “Advanced USC Power Generation Technology”, Journal of the Japan Society of Mechanical Engineers, Vol. 114, No. 1109 (2011), pp. 22-25.

[2] Kjaer, S., Klauke, F., Vanstone, R., Zeijseink, A., Weissinger, G., Kristensen, P., Meier, J., Blum, R and Wieghardt, K., “The advanced Supercritical 700℃ Pulverised Coal-Fired Power Plant”, VGB Power Technology, Vol. 82, No. 7 (2002), pp. 46-49.

[3] Zhao, S., Xie, X., Smith, G.D and Patel, S.J., “Research and Improvement on Structure Stability and Corrosion Resistance of Nickel-Base Superalloy INCONEL Alloy 740,” Materials and Desigh, Vol.27 (2006), pp.1120-1127.

[4] Patel, S.J., “Introduction to Inconel Alloy 740: an Alloy Designed for Superheater Tubing in Coal-Fired Ultra Supercritical Boilers”, Acta Metallurgica Sinica (English Letters), Vol. 18, No. 4 (2005), pp. 479-488.

[5] Klower, J., Husemann, R.U. and Bader, M., “Development of Nickel Alloys Based on Alloy 617 for Components in 700°C Power Plant”, Procedia Engineering, No. 55 (2013), pp.226-231.

[6] Zhao, S., Xie, X., Smith, G.D and Patel, S.J., “Microstructural Stability and Mechanical Properties of a New Nickel-Based Superalloy”, Materials Science and Engineering A, Vol. 355 (2003), pp.96-243.

[7] Evans, N.D., Maziasz, P.J., Swindeman, R.W and Smith, G.D., “Microstructure and Phase Stability in INCONEL Alloy 740 during Creep”, Scripta Materialia, Vol. 51 (2004), pp. 503-507.

[8] Guo, Y., Wang, B. and Hou, S., “Aging Precipitation Behavior and Mechanical Properties of Inconel 617 Superalloy”, Acta Metallurgica Sinica, Vol.26, No.3 (2013), pp.307-312.

[9] Rahman, M., Priyadarshan, G. Raja, K.S., Nesbitt, C. and Misra, M., "Characterization of High Temperature Deformation Behavior of INCONEL 617", Mechanics of Materials, No. 41 (2009), pp.261-270.
[10] Knezevic, V., Schneider, A. and Landier, C., "Creep Behavior of Thick-wall Alloy 617 Seamless Pipes for 700°C Power Plant Technology", Procedia Engineering, No. 55 (2013), pp.240-245.
[11] Klenk, A., Speicher, M. and Maile, K., "Weld behavior of Martensitic Steels and Ni-based Alloys for High Temperature Components", Procedia Engineering, No. 55 (2013), pp.414-420.
[12] Zhang, S. and Takahashi, Y., "Evaluation of Creep Deformation and Rupture Behavior of Alloy 740H and Alloy 617 – Investigation using Smooth and Circumferential Notched Bar Specimens", CRIEPI report, Q14011 (2015, in Japanese).
[13] Takahashi, Y., "Evaluation of Creep-Fatigue Life Prediction Methods for Low-Carbon Nitrogen-Added 316 Stainless Steel", Transactions of the ASME, Journal of Engineering Materials and Technology, Vol.120 (1998), pp.119-124.
[14] Takahashi, Y., "Study on Creep-Fatigue Evaluation Procedures for High-Chromium Steels – Part I: Test result and Life Prediction Based on Measured Stress Relaxation", International Journal of Pressure Vessels and Piping, Vol.85 (2008), pp.406-422.
[15] Takahashi, Y., Shibamoto, H. and Inoue, K., "Study on Creep-Fatigue Life Prediction Methods for Low-Controlled 316 Stainless Steel (316FR)", Nuclear Engineering and Design, Vol.238 (2008), pp.322-335.
[16] American Society of Mechanical Engineers, Boiler and Pressure Vessel Code Section III, Division 1, Subsection NH (1995).
[17] Hales, R., "A Method of Creep Damage Summation Based on Accumulated Strain for the Assessment of Creep-Fatigue Endurance", Fatigue of Engineering Materials and Structures, Vol. 6, No.2 (1983), pp.121-135.
[18] Takahashi, Y., Dogan, B. and Gandy, D., "Systematic Evaluation of Creep-Fatigue Life Prediction Methods for Various Alloys", Journal of Pressure Vessels Technology, Vol.135 (2013), pp. (061204-1)-(061204-10).